



Contents lists available at ScienceDirect

Spectrochimica Acta Part A: Molecular and Biomolecular Spectroscopy

journal homepage: www.elsevier.com/locate/saa

Artificial neural network modeling of photocatalytic removal of a disperse dye using synthesized ZnO nanoparticles on montmorillonite

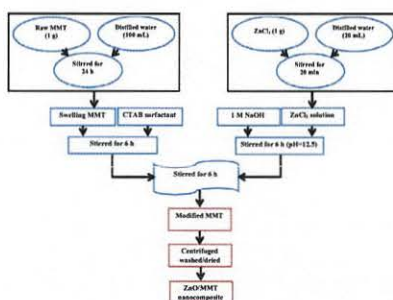
Murat Kıranşan^a, Alireza Khataee^{b,*}, Semra Karaca^{a,*}, Mohsen Sheydaei^b^a Department of Chemistry, Faculty of Science, Atatürk University, 25240 Erzurum, Turkey^b Research Laboratory of Advanced Water and Wastewater Treatment Processes, Department of Applied Chemistry, Faculty of Chemistry, University of Tabriz, Tabriz, Iran

HIGHLIGHTS

- Synthesis and immobilization of zinc oxide nanoparticles on montmorillonite.
- Characterization of the ZnO/MMT nanocomposite by XRD, SEM, TEM, and BET.
- Photocatalysis of a disperse dye by synthesized ZnO/MMT nanocomposite.
- ANN modeling of the effect of the ZnO/MMT/UV-C process in removal of the dye.

GRAPHICAL ABSTRACT

Schematics of synthesis of ZnO nanoparticles on montmorillonite.



ARTICLE INFO

Article history:

Received 30 September 2014

Received in revised form 11 November 2014

Accepted 28 December 2014

Available online 14 January 2015

Keywords:

Artificial neural network
Photocatalytic degradation
ZnO nanoparticles
ZnO/MMT nanocomposite

ABSTRACT

In this study, the photocatalytic ability of ZnO/Montmorillonite (ZnO/MMT) nanocomposite under UV-A, UV-B and UV-C radiation was investigated. ZnO nanoparticles were synthesized on the surface of MMT and used as photocatalyst in decolorization of Disperse Red 54 (DR54) solution. Synthesized nanocomposite was characterized by X-ray diffraction (XRD), scanning electron microscopy (SEM), transmission electron microscopy (TEM) techniques and nitrogen adsorption/desorption isotherms curves. The average width of synthesized ZnO particles is in the range of 30–45 nm. Effect of UV light regions, initial dye concentration, initial dosage of nanocomposite, and reusability of catalyst was studied on decolorization efficiency. The highest decolorization efficiency was achieved under UV-C radiation. A three-layered feed forward back propagation artificial neural network model was developed to predict the photocatalysis of DR54 under UV-C radiation. According to ANN model the ZnO/MMT dosage with a relative importance of 49.21% is the most influential parameter in the photocatalytic decolorization process.

© 2015 Elsevier B.V. All rights reserved.

Introduction

Heterogeneous photocatalytic oxidation process, as an advanced oxidation process, has been widely applied and occupied

an important place in the field of water and wastewater treatment over the past few decades [1,2]. The photochemical reactions relied on the in-situ generation of hydroxyl radicals ($\cdot\text{OH}$) employing semiconductor photocatalyst such as TiO_2 and ZnO, and an energetic radiation source like UV light is considered as promising process for degradation of persistent organic pollutants such as herbicides, pesticides and dyes [3–5].

Heterogeneous photocatalyst has moderate energy band-gap between its valence and conduction bands [6]. The absorption of

* Corresponding authors. Tel.: +98 411 3393165; fax: +98 411 3340191 (A. Khataee). Tel.: +90 442 2314435; fax: +90 442 2360948 (S. Karaca).

E-mail addresses: a_khataee@tabrizu.ac.ir, ar_khataee@yahoo.com (A. Khataee), skaraca@atauni.edu.tr, semra_karaca@yahoo.com (S. Karaca).

photons with energy equal to or greater than its band gap leads to promotion of electron from valence band to the conduction band and yields hole (h^+)/electron (e^-) pairs. The developed e^- and h^+ may migrate to the catalyst surface where they participate in decomposition of pollutants through redox reactions [7]. The e^- may react with O_2 to form $\cdot O_2^-$ and the h^+ may react with either H_2O or OH^- adsorbed on the catalyst surface to generate $\cdot OH$. Photocatalytic decomposition of pollutants usually involves reaction of pollutant with photogenerated reactive radicals or direct attack from the h^+ [1].

Application of heterogeneous photocatalysis in degradation of organic pollutants offers several advantages: (1) most of the popular photocatalysts are inexpensive and can be found abundantly, (2) photocatalytic degradation operates at ambient conditions (atmospheric O_2 is used as oxidant), (3) no other post treatment and chemical reagent are needed and (4) the mineralization products are mainly non-toxic byproducts such as H_2O , CO_2 , and mineral acids [8,9].

However some problems associated with suspended photocatalytic particles. Separation of used particles after water treatment is one of these basic problems [10]. In order to settle the problems related to the use of photocatalyst powder, many researchers made efforts to immobilize the catalysts in different ways. Photocatalyst powder can be immobilized on inert solid substrates such as activated carbon, clinoptilolite and glass media [11–13].

In this work, ZnO/montmorillonite nanocomposite was prepared and its pore structure, crystalline structures and particle sizes were characterized. The performance of prepared nanocomposite for adsorption and photocatalytic degradation of an organic pollutant under UV-A, UV-B or UV-C light was investigated. Disperse Red 54 (DR54) was selected as model pollutant which is an azo dyestuff popularly seen in the textile wastewater. Effect of UV light region, initial dye concentration, and initial dosage of nanocomposite variables on decolorization efficiency was investigated. An artificial neural network model (ANN) was developed to predict the photocatalysis of DR54.

Experimental procedure

Materials

C.I. Disperse Red 54 was procured from Berşan textile Co. (Turkey). Characteristics and chemical structure of this dye are shown in Table 1. $ZnCl_2$, HCl and NaOH were purchased from Merck Co. (Germany). Montmorillonite K10 (MMT) was purchased from Sigma–Aldrich Co. (USA) which consists of SiO_2 , Al_2O_3 , Fe_2O_3 , MgO, CaO, Na_2O , and K_2O with 66.9, 13.8, 2.8, 1.6, 0.3, 0.2 and 1.7 wt.%, respectively. Cetyltrimethylammonium bromide (CTAB) was purchased from Sigma–Aldrich Co. (USA). All other chemicals were of analytical grade. Distilled water was used throughout the investigation.

Catalysts synthesis and characterization

ZnO/MMT nanocomposite was prepared through synthesis of ZnO nanoparticles and their immobilization on the surface of the MMT. Accordingly, 1 g of $ZnCl_2$ was dissolved in 20 mL of distilled water. 1 M sodium hydroxide solution was added dropwise to the solution to obtain an alkaline medium (pH = 12.50). Simultaneously, 1 g MMT was homogeneously dispersed in 100 mL distilled water and a desired amount of CTAB was slowly added to suspension. The concentration of surfactant was 1.0 CEC of pure MMT. The $ZnCl_2$ solution was added to the prepared CTAB/MMT suspension and the prepared mixture was stirred for 6 h. The sample was washed and centrifuged with distilled water to remove any

non-adhesive impurities, and then dried at 90 °C for 3 h to remove moisture. Pure ZnO nanoparticles were synthesized by the same procedure described for the synthesis of the ZnO/MMT nanocomposite without addition of the MMT.

Scanning electron microscope (SEM) model MIRA3 FEG-SEM Tescan (Czech) was used to characterize the structure and morphology of MMT particles and ZnO/MMT composite.

For transmission electron microscopy (TEM) observations, the synthesized ZnO/MMT sample was dispersed in the ethanol using ultrasonic vibration (Sonorex Bandelin Digi Tec, UK) for 15 min, and then a drop of dispersed sample was placed on a copper grid coated with a layer of amorphous carbon. TEM images were recorded by a Cs-corrected high-resolution TEM (Zeiss-EM10C, Germany) operated at 100 kV. X-ray diffraction (XRD) patterns were obtained at room temperature by PANalytical X'Pert PRO diffractometer (Germany) using $Cu-K\alpha$ radiation ($\lambda = 1.5406 \text{ \AA}$). Textural properties of the MMT, ZnO and ZnO/MMT samples were determined from N_2 adsorption/desorption isotherms at 77 K on a Gemini 2385 nitrogen adsorption apparatus (Micromeritics Instruments, USA) and their pore structure analyzed using Brunauer–Emmett–Teller (BET), t -Plot and Barrett–Joyner–Halenda (BJH) equations.

Decolorization setup and procedure

The experimental reactor used for the adsorption and photocatalytic degradation of DR54 is consisted of 900 mL cylindrical vessel with working volume of 500 mL equipped with a UV-A, UV-B or UV-C lamp (8 W, Herolab, Germany) as the light source (Fig. 1). The solution in the reactor was constantly stirred via a magnetic stirrer.

In a typical photocatalytic run, 500 mL of the aqueous solution containing the desired concentration of DR54 in the range 40–120 mg/L and 0.0625–0.9 g of the as-prepared nanocomposite were loaded in the reaction vessel. The UV-A, UV-B or UV-C lamp was turned on while the suspension was magnetically stirred. At a defined time interval, about 5 mL of the solution was withdrawn from the suspension. Concentration of DR54 in solutions was measured photometrically using Varian Cary 100 UV–Vis spectrophotometer (Australia). Prior to the measurement, the UV–Vis spectra of DR54 solution were recorded from 200 nm to 800 nm. The maximum absorbance wavelength of DR54 was at 460 nm. After determination of DR54 concentration versus time, the decolorization efficiency (%) was calculated through Eq. (1):

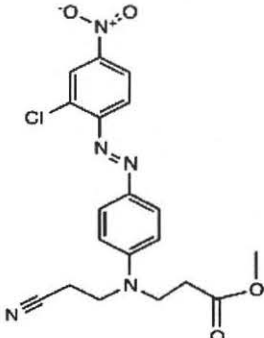
$$\text{Decolorization efficiency (\%)} = \frac{C_0 - C_t}{C_0} \times 100 \quad (1)$$

where C_0 and C_t are concentration of the dye initially and at time t , respectively. Adsorption experiments were done using the method applied for photocatalytic degradation experiment without UV radiation.

Artificial neural network (ANN) as a comprehensive technique to model complex processes was used to predict the effects of the initial concentration of DR54, nanocomposite dosage and radiation time on decolorization efficiency of photocatalytic degradation process under UV-C radiation. The ANN model in this work is consisted of three input, hidden and output layers. The layers, number of neurons as processing unit of ANN in each layer, and the transfer functions between layers form neural network topology [14]. The linear transfer function was used in hidden and output layers. The range of initial concentration of DR54, nanocomposite dosage and radiation time as input layers was 40–120 mg/L, 0.0625–0.9 g/L and 5–120 min, respectively and decolorization efficiency as output layers was between 73.58–99.92%. All values were normalized in the 0.1–0.9 range as follows:

$$X_i = \frac{0.8(X_i - X_{\min})}{(X_{\max} - X_{\min})} + 0.1 \quad (2)$$

Table 1
Characteristics of C.I. Disperse Red 54.

| C.I. name | Chemical structure | Molecular formula | M_w (g/mol) | λ_{max} (nm) | Class |
|-------------------------|---|------------------------|---------------|----------------------|---------|
| Disperse Red 54 (DR 54) |  | $C_{19}H_{18}ClN_5O_4$ | 415.83 | 460 | Monoazo |

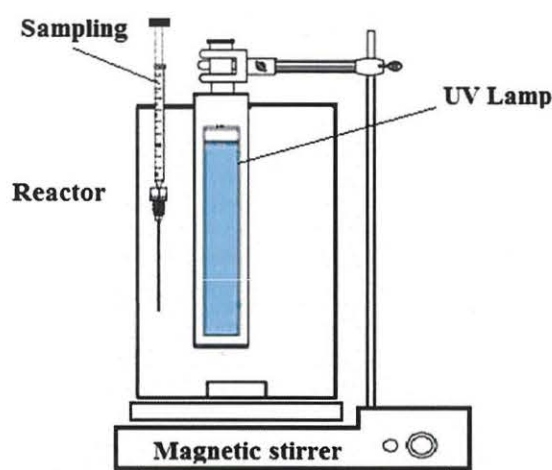


Fig. 1. Schematic of the experimental reactor used for decolorization of DR54 solution.

where x_i , X_i , X_{min} and X_{max} are normalized value (i is an index of data), actual experimental value, minimum and maximum actual experimental values of data sets, respectively.

Results and discussion

Characterization of the synthesized ZnO/MMT nanocomposite

The SEM images of the MMT and ZnO/MMT samples are illustrated in Fig. 2. Comparing SEM images of the MMT (Fig. 2a) and the ZnO/MMT (Fig. 2b) samples indicates the immobilization of fine ZnO particles on the surface of MMT. The average width of produced structures is determined using Manual Microstructure Distance Measurement software (Nahamin Pardazan Asia Co., Iran). The average width of synthesized particles is in the range of 30–45 nm (Fig. 2c). The EDX microanalyses (wt.%) of the prepared ZnO/MMT nanocomposites confirmed the coexistence of C, O, Zn, Al, Si and K in the composite. Comparison the constituents of ZnO/MMT nanocomposites with those of pristine MMT approved the immobilization of ZnO nanoparticles on the surface of MMT in ZnO/MMT nanocomposite sample.

In order to have more precise estimation about the particle size of the ZnO particles in the ZnO/MMT, TEM images of this nanocomposite was recorded (Fig. 3). The TEM images show the immobilization

of ZnO nanoparticles with average size <50 nm on the surface of the MMT approving the results obtained from SEM analysis.

XRD pattern of the ZnO/MMT (patterns are not shown) displayed distinct peaks at 2θ values of about 31.71, 34.41, 36.21, 47.51, 56.61, 63.0, 66.08, 68.0, 68.28, 71.64, and 75.96° which are respectively reflected by typical ZnO planes of (100), (002), (101), (102), (110), (103), (200), (112), (201), (004), and (202) planes of ZnO, respectively (JCPDS Card 36-1451), [15] and the peak at 2θ value of 26.5° corresponds to the interlayer spacing of MMT [16]. The results indicate the development of ZnO/MMT nanocomposite through synthesis of ZnO nanoparticles on the MMT.

Fig. 4 shows the nitrogen adsorption/desorption isotherms curves for ZnO, MMT and ZnO/MMT samples. It could be seen that ZnO and ZnO/MMT were type IV according to the acknowledged BDDT classification and each had a hysteresis loop that was representative of mesoporous structure [17].

The nitrogen adsorption/desorption on the MMT sample obey type II isotherm with hysteresis loops indicating that the sample are relatively strong adsorbent and the sample has a mesoporous texture containing open slit-shaped capillaries [17–19].

Result obtained from analysis of nitrogen adsorption/desorption isotherms with BET, t -Plot and BJH equations are reported in Table 2. Comparison of these results indicates that immobilization of ZnO on the surface of MMT leads to production of nanocomposite with higher surface area and pore volume than those of pure ZnO.

Photocatalytic decolorization process

Effect of initial dye concentration

To determine the desired conditions of the photocatalytic degradation process, effect of initial concentration of DR54, nanocomposite dosage and UV radiation variables on decolorization efficiency was tested. The role of the initial dye concentration on decolorization was investigated and the results are shown in Fig. 5. According to the obtained results in ZnO/MMT/UV-C process when the initial concentration was 40 mg/L, the dye was almost decolorized after 15 min. With increase in dye concentration from 40 to 120 mg/L, the decolorization efficiency decreased. The decrease in decolorization efficiency with increasing the initial dye concentration can be attributed to decrease the path length of photon entering the dye solution and consequently decrease in generation of $\cdot OH$ [20]. Simultaneously, the presence of additional dye molecules adsorbed on the surface of ZnO/MMT affects the photocatalytic performance of nanocomposite. Muruganandham et al. also reported the similar trend in the photocatalytic degradation of reactive yellow 14 by TiO_2 particles [21].

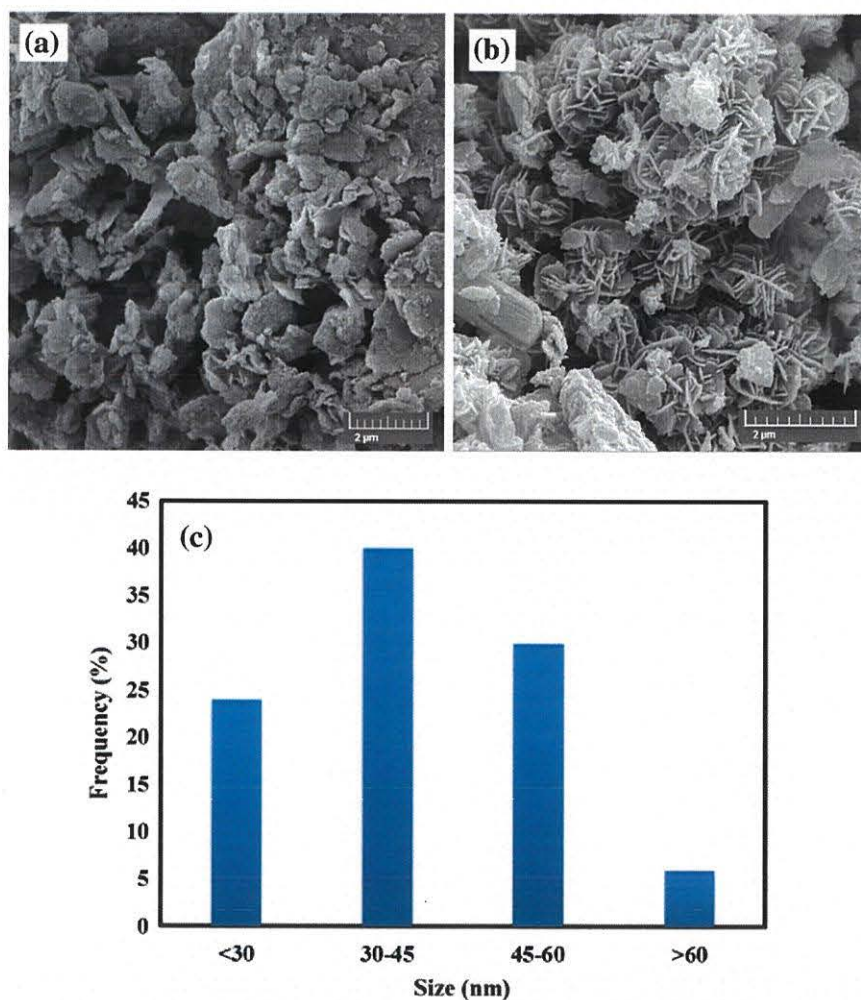


Fig. 2. SEM images of (a) pristine MMT and (b) modified ZnO/MMT, along with (c) distribution of ZnO particles size in ZnO/MMT sample.

Langmuir–Hinshelwood (L–H) model was used to evaluate kinetic behavior of the reaction occurring at the heterogeneous catalytic surface and describe the influence of the initial concentration of DR54 on the photocatalytic decolorization rate through the Eq. (3) [22]:

$$\frac{1}{k_{app}} = \frac{1}{k_c k_{ads}} + \frac{C_0}{k_c} \quad (3)$$

where C_0 is the initial concentration of DR54, k_{app} is apparent pseudo-first-order constant (1/min), k_c is the reaction rate constant (mg/L min), and k_{ads} is the adsorption rate constant (L/mg). Values of $\ln(C_0/C)$ were plotted versus time. The slopes of linear regressions were k_{app} . The variations of $1/k_{app}$ as a function of initial concentration of dye are given in Fig. 6. The regression coefficient was 0.985, which suggested the photodegradation of DR54 by the ZnO/MMT fits the Langmuir–Hinshelwood kinetic model. k_c and k_{ads} were estimated as 0.174 mg/L min and 0.133 L/mg, respectively. Daneshvar et al. reported a Langmuir–Hinshelwood equation constant of $k_c = 0.209$ mg/L min and $k_{ads} = 0.124$ L/mg for the photocatalytic degradation of diazinon in the presence of ZnO nanopowder [23]. For photocatalytic reduction of Cr^{6+} over ZnO-Kaolin nanocomposite, the values of k_c and k_{ads} were reported as 0.321 mg/L min and 0.118 L/mg, respectively by Shirzad-Siboni et al. [24]. k_c and k_{ads} values of respectively 1.99 mg/L min and 0.354 L/mg were reported by Daneshvar et al. for photocatalytic removal of C.I. Acid

Orange 7 from aqueous solution [5]. Comparing of the estimated values of Langmuir–Hinshelwood kinetic constants of this work with literature indicates that both reaction rate and adsorption rate constants for the photocatalysis of DR54 in the presence of the ZnO/MMT nanocomposite is appropriate.

Effect of ZnO/MMT dosage

Photocatalyst dosage is an important parameter in photocatalytic reactions. Therefore, the effect of initial ZnO/MMT nanocomposite on the decolorization efficiency of 100 mg/L DR54 solution under UV-C radiation was investigated with ZnO/MMT dosage of 0.0625–0.9000 g/L. The effect of catalyst loading on the percent decolorization of DR54 is shown in Fig. 7. It can be observed that the decolorization efficiency of dye solution increases with increasing ZnO/MMT dosage from 0.0625 to 0.7500 g/L. This is due to the increasing active sites for photocatalytic generation of reactive radicals and dye molecules adsorption on the surface of ZnO/MMT to effective degradation [25,26]. However, further increase in the nanocomposite dosage leads to decrease in decolorization efficiency. This decrease is because of increase in the opacity of DR54-ZnO/MMT suspension which suppresses the effective UV light penetration [22,27].

Effect of UV radiation region

The effect of UV light on degradation of dyes using the ZnO/MMT catalyst was investigated at three UV light region, covering

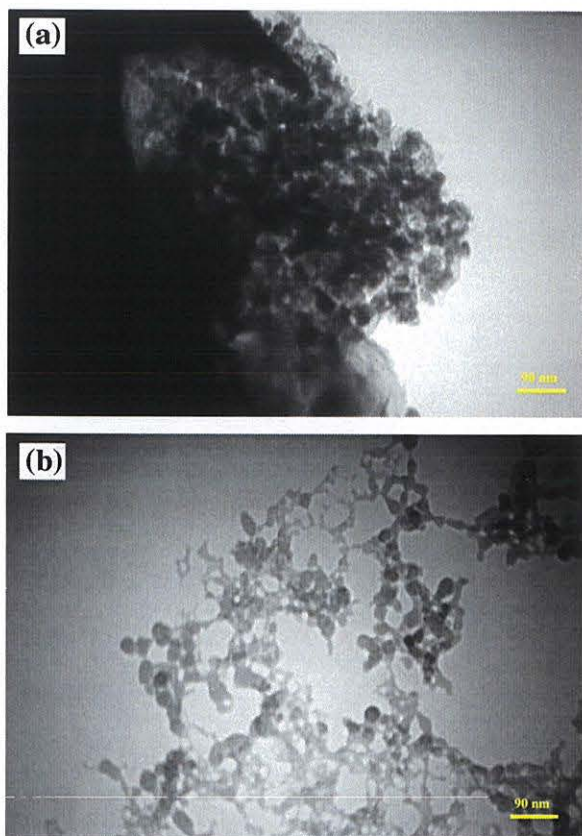


Fig. 3. TEM images of ZnO/MMT nanocomposite.

the UV-A (315–400 nm), UV-B (280–315 nm) and UV-C (200–280 nm). Decolorization efficiency of DR54 solution using ZnO/MMT nanocomposite in the absence and presence of UV-A, UV-B or UV-C lights was shown in Fig. 8. The decolorization efficiency of dye was increases in the order of without radiation < UV-A < UV-B < UV-C. Energy of photons emitted from UV-C lamp was higher than that of UV-B and UV-A. Therefore photogeneration of e^-/h^+ pairs under UV-C radiation was higher and consequently more reactive radicals were developed for degradation of pollutant.

Table 2

Surface area and porosity characteristics of ZnO, MMT and ZnO/MMT nanocomposite samples.

| Sample | ZnO | MMT | ZnO/MMT |
|------------------------------------|-------------|-------------|-------------|
| Specific surface area (m^2/g) | 38.22 | 279.28 | 70.54 |
| Micropore surface area (m^2/g) | 1.9924 | 6.6703 | – |
| Mesopore surface area (m^2/g) | 32.45 | 285.55 | 84.98 |
| Micropore volume (cm^3/g) | 0.000816 | 0.000335 | 0.0000 |
| Total pore volume (cm^3/g) | 0.217–0.277 | 0.416–0.428 | 0.213–0.228 |

Effect of ZnO immobilization on MMT

The comparison of the ability of ZnO and ZnO/MMT on decolorization of DR54 aqueous solution in photocatalytic degradation processes under UV-C radiation, with and without catalyst is presented in Fig. 9. Obtained results indicate that immobilization of ZnO on the surface of MMT leads to increase in its photocatalytic performance under all investigated UV radiations. This can be attributed to increased surface area of ZnO/MMT rather than ZnO which leads to increase in adsorption of H_2O/OH^- and pollutant to the surface of photocatalyst. More adsorption of H_2O/OH^- leads to develop more reactive radicals through reaction with photogenerated h^+ and more adsorption of pollutant to the surface of photocatalyst where reactive radicals are developed.

ANN modeling

In order to determine the optimum topography to model the DR54 decolorization process, a series of topologies was used in which the number of neurons in the hidden layer was varied from 2 to 20. The mean square error (MSE) was performed to investigate the relation between the neurons in the hidden layer and network error. According to the obtained results shown in Fig. 10, MSE decreases with increasing hidden neuron sizes and then decreased when the number of hidden neurons is greater than 10. Accordingly, optimal value of the number of input, hidden and output layers of respectively, 5, 10 and 1 was selected as optimum topography to model the DR54 decolorization process. Set of connection weights and biases that cause the optimum ANN topography are listed in Table 3.

The formulated ANN model was tested for its validity by comparison the model-predicted values of decolorization efficiency of test set with those obtained from the corresponding experiments. Comparison between these values was shown in Fig. 11. Obtained correlation coefficient (R^2) of the line shows the good performance of ANN model in prediction of experimental data within adopted

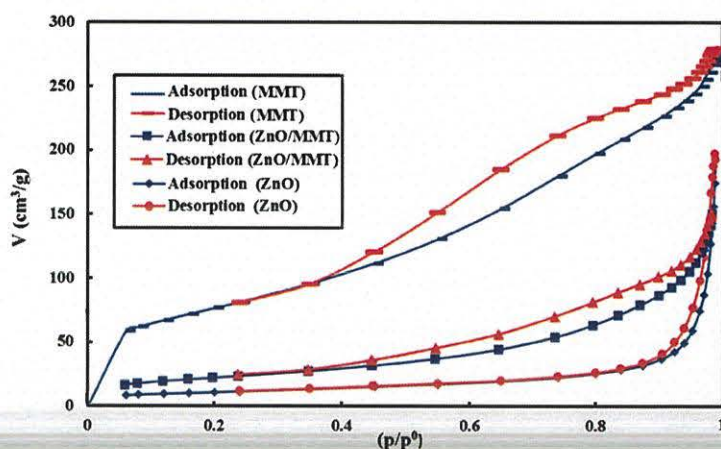


Fig. 4. Nitrogen adsorption/desorption isotherm curves for ZnO, MMT and ZnO/MMT samples.

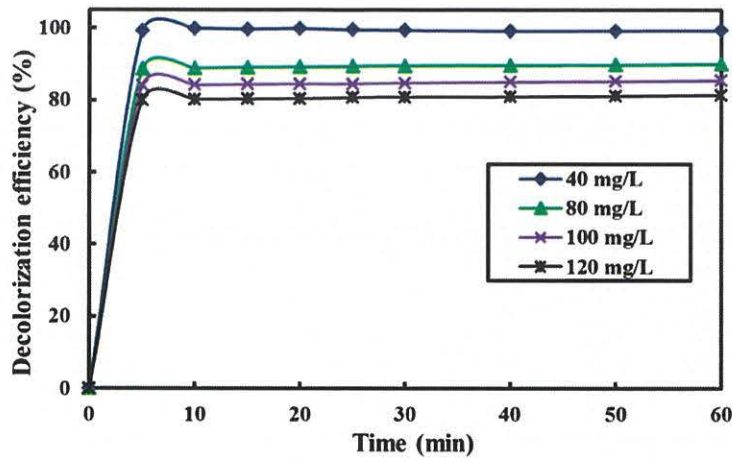


Fig. 5. Effect of DR54 initial concentration on the decolorization of the dye solution (experimental conditions: [catalyst]₀ = 0.750 g/L under UV-C radiation).

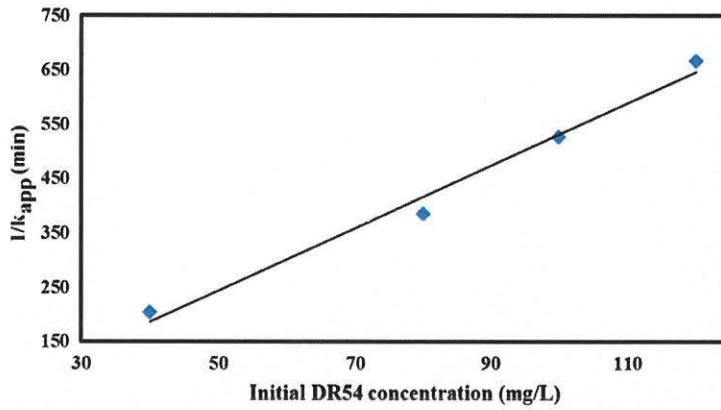


Fig. 6. Variations of 1/k_{app} as a function of initial concentration of DR54.

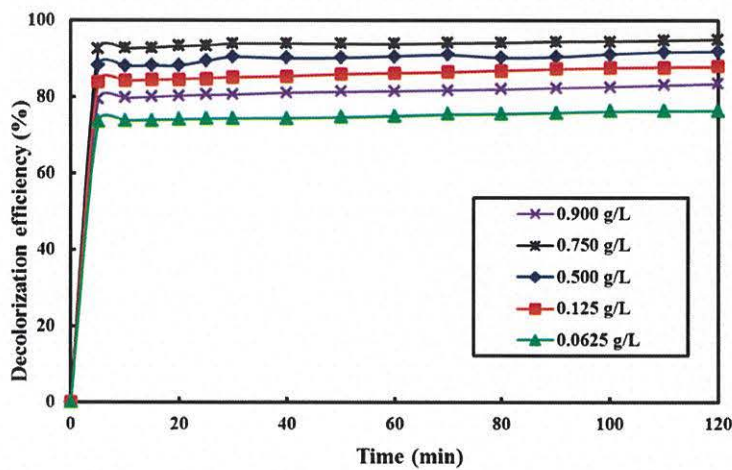


Fig. 7. Effect of ZnO/MMT dosage on the decolorization of DR54 (experimental conditions: [DR54]₀ = 100 mg/L under UV-C radiation).

ranges. The relative effect of ZnO/MMT dosage, UV radiation time and initial concentration of DR54 on decolorization efficiency (%) was calculated by Eq. (4):

$$I_j = \frac{\sum_{m=1}^{m=N_h} (|W_{jm}^{ih}| / \sum_{k=1}^{k=N_i} |W_{km}^{ih}|) \times |W_{mn}^{ho}|}{\sum_{k=1}^{k=N_i} \{ \sum_{m=1}^{m=N_h} (|W_{jm}^{ih}| / \sum_{k=1}^{k=N_i} |W_{km}^{ih}|) \times |W_{mn}^{ho}| \}} \quad (4)$$

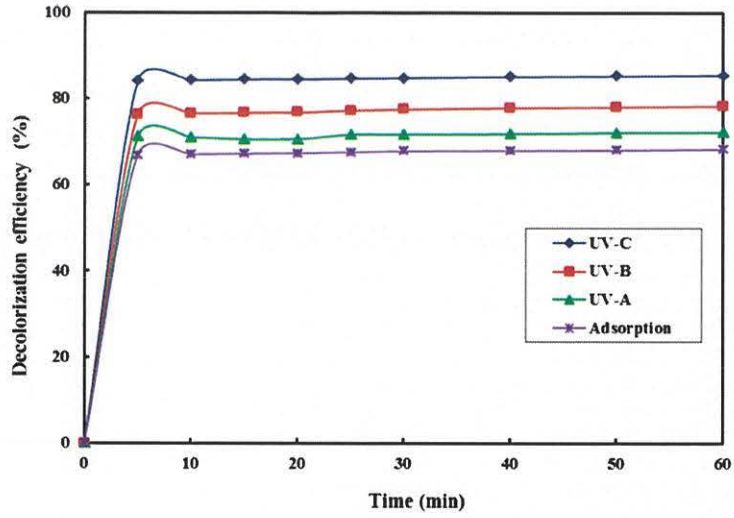


Fig. 8. Effect of UV radiation region on the decolorization of DR54 (experimental conditions: $[DR54]_0 = 100 \text{ mg/L}$, and $[catalyst]_0 = 0.750 \text{ g/L}$).

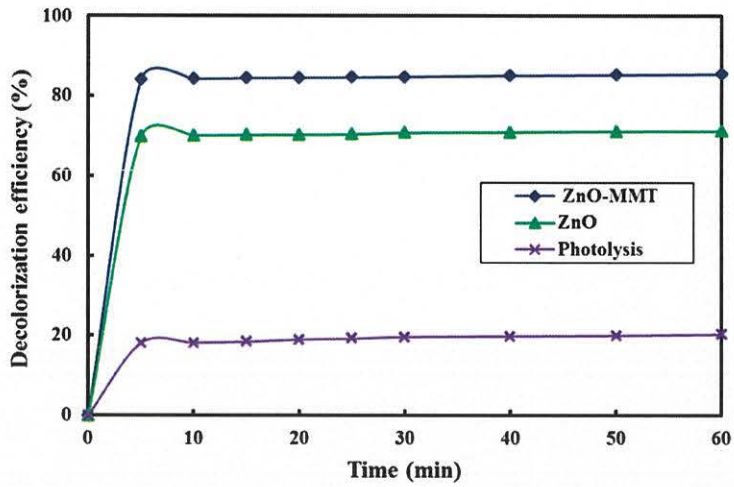


Fig. 9. Comparison ability of ZnO/MMT/UV-C, ZnO/UV-C and UV-C in degradation of DR54 solution (experimental conditions: $[DR54]_0 = 100 \text{ mg/L}$, and $[catalyst]_0 = 0.750 \text{ g/L}$).

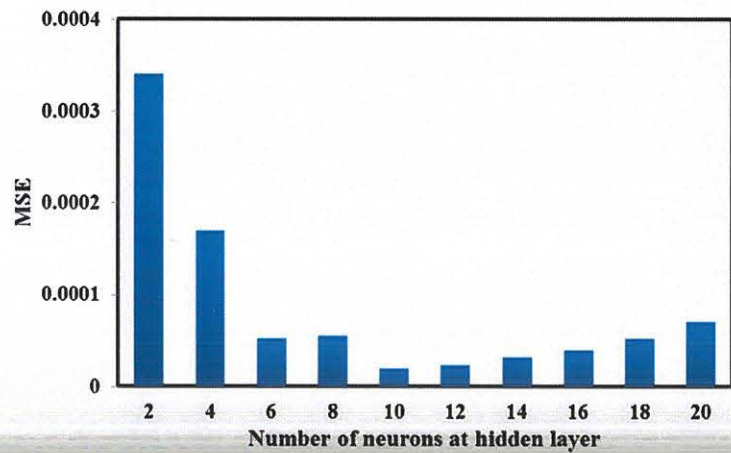


Fig. 10. Dependence between MSE and number of neurons at hidden layer.

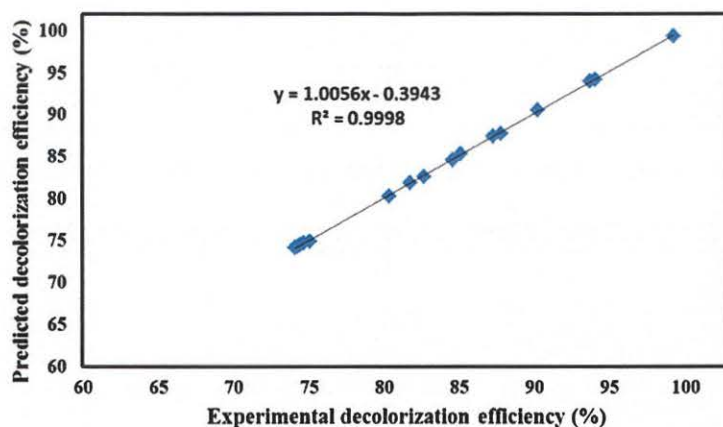


Fig. 11. Predicted result vs. experimental result for decolorization efficiency.

Table 3
Matrices of ANN optimized structure weights.

| Weights and biases between input and hidden layers | | | | |
|--|----------------|-------------------|-------------------------------|---------|
| Neuron of hidden layer | Variable | | | Bias |
| | ZnO/MMT dosage | UV radiation time | Initial concentration of DR54 | |
| 1 | 1.2985 | 1.5312 | 1.3424 | 3.6598 |
| 2 | 2.216 | 0.5766 | 3.9096 | 1.803 |
| 3 | 2.7334 | 0.65166 | 1.252 | 2.3063 |
| 4 | 0.098635 | 1.9964 | 0.55546 | 1.8075 |
| 5 | 2.3875 | 1.1643 | 1.9046 | 1.3888 |
| 6 | 0.84627 | 1.3953 | 2.4171 | 0.71036 |
| 7 | 0.559 | 0.32624 | 1.3131 | 1.1461 |
| 8 | 4.9932 | 0.18984 | 1.9427 | 4.1124 |
| 9 | 4.5481 | 0.78314 | 0.99988 | 5.9675 |
| 10 | 2.7109 | 1.4352 | 1.7251 | 2.9187 |
| Weights and bias between hidden and output layers | | | | |
| Neuron of hidden layer | Weights | | | Bias |
| 1 | 0.27442 | | | 2.4879 |
| 2 | 0.4651 | | | |
| 3 | 0.38144 | | | |
| 4 | 0.23946 | | | |
| 5 | 0.22111 | | | |
| 6 | 0.42797 | | | |
| 7 | 2.1344 | | | |
| 8 | 1.548 | | | |
| 9 | 3.4744 | | | |
| 10 | 0.8931 | | | |

where I_j , W and N are the relative importance of the j th input variable on the decolorization efficiency, connection weight, and the numbers neurons, respectively, the subscripts ' k ', ' m ' and ' n ' refer to input, hidden and output neurons, respectively and the superscripts ' i ', ' h ' and ' o ' refer to input, hidden and output layers, respectively. Obtained results show that the relative importance ZnO/MMT dosage, UV radiation time and initial concentration of DR54 on decolorization efficiency were 49.21%, 21.01% and 29.78%, respectively.

Regeneration of ZnO/MMT

The stability and reusability of a photocatalyst had significant impact on its performance in photocatalytic degradation processes, hence made the application of the materials more economical. Here, decolorization of 100 mg/L DR54 solution was conducted in the presence of ZnO/MMT of 0.75 g/L under UV-C radiation. Then

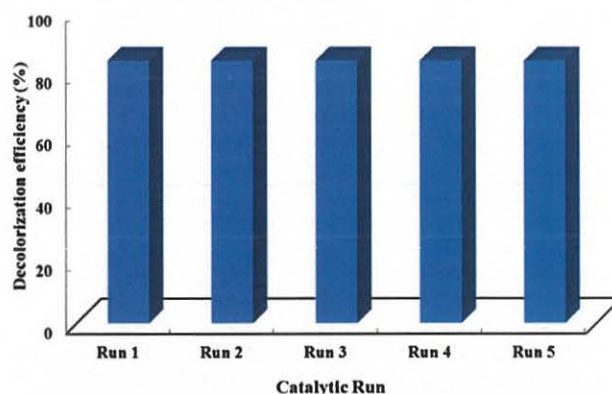


Fig. 12. Reusability behavior of ZnO/MMT in photocatalytic degradation process (experimental conditions: $[DR54]_0 = 100$ mg/L, and $[catalyst]_0 = 0.750$ g/L under UV-C radiation).

the ZnO/MMT was separated from treated wastewater, washed with distilled water and dried to use for another photocatalytic degradation cycle keeping the concentration of dye and dosage of photocatalyst constant. As shown in Fig. 12 even after five cycles, no remarkable change in the decolorization efficiency was observed indicating the stability of the ZnO/MMT nanocomposite in successive photocatalytic degradation processes.

Conclusions

The results of the present study showed that the immobilization of ZnO nanoparticles on the surface of MMT is an effective method to enhance its photocatalytic performance under whole UV radiation regions. Increasing the ZnO/MMT dosage and decreasing initial concentration of dye could enhance the decolorization efficiency. Photocatalytic performance of ZnO/MMT under UV-C radiation was higher than that under UV-B and UV-A radiation. According to the results of ANN modeling, effect of ZnO/MMT dosage on decolorization efficiency was higher than that of UV radiation time and initial concentration of DR54. The ZnO/MMT nanocomposite is stable photocatalyst and appropriate for long-time application.

Acknowledgments

The authors thank to TUBITAK for supports by the 2221-Fellowship Program for Visiting Scientists and Scientists on Sabbatical

Leave. The authors also thank the Atatürk University of Erzurum (Turkey) and University of Tabriz (Iran) for all of the support provided.

References

- [1] A.R. Khataee, M. Safarpour, M. Zarei, S. Aber, *J. Mol. Catal. A: Chem.* 363–364 (2012) 58–68.
- [2] B. Ayoubi-Feiz, S. Aber, A. Khataee, E. Alipour, *Environ. Sci. Pollut. Res.* 21 (2014) 8555–8564.
- [3] R. Pourata, A.R. Khataee, S. Aber, N. Daneshvar, *Desalination* 249 (2009) 301–307.
- [4] A.R. Khataee, M. Zarei, M. Fathinia, M.K. Jafari, *Desalination* 268 (2011) 126–133.
- [5] N. Daneshvar, M.H. Rasoulifard, A.R. Khataee, F. Hosseinzadeh, *J. Hazard. Mater.* 143 (2007) 95–101.
- [6] A. Cuzzola, M. Bernini, P. Salvadori, *Appl. Catal. B* 36 (2002) 231–237.
- [7] R. Saleh, N.F. Djaja, *Spectrochim. Acta Part A* 130 (2014) 581–590.
- [8] U.G. Akpan, B.H. Hameed, *J. Hazard. Mater.* 170 (2009) 520–529.
- [9] W. Zhang, L. Zou, L. Wang, *Appl. Catal. A Gen.* 371 (2009) 1–9.
- [10] Y. Hou, J. Qu, X. Zhao, P. Lei, D. Wan, C.P. Huang, *Sci. Total Environ.* 407 (2009) 2431–2439.
- [11] A.R. Khataee, M.N. Pons, O. Zahraa, *J. Hazard. Mater.* 168 (2009) 451–457.
- [12] D. Rajamanickam, M. Shanthi, *Spectrochim. Acta Part A* 128 (2014) 100–108.
- [13] A. Nezamzadeh-Ejhieh, S. Khorsandi, *J. Ind. Eng. Chem.* 20 (2014) 937–946.
- [14] A.R. Khataee, M. Zarei, M. Pourhassan, *CLEAN – Soil Air, Water* 38 (2010) 96–103.
- [15] A. Khataee, R. Darvishi Cheshmeh Soltani, Y. Hanifehpour, M. Safarpour, H. Gholipour Ranjbar, S.W. Joo, *Ind. Eng. Chem. Res.* 53 (2014) 1924–1932.
- [16] F. Rasouli, S. Aber, D. Salari, A.R. Khataee, *Appl. Clay Sci.* 87 (2014) 228–234.
- [17] W. Liu, P. Yin, X. Liu, X. Dong, J. Zhang, Q. Xu, *Chem. Eng. Res. Des.* 91 (2013) 2748–2758.
- [18] S.J. Gregg, K.S.W. Sing, *Adsorption, Surface Area, and Porosity*, 2nd ed., Academic Press, London, New York, 1982.
- [19] F.O. Rouquerol, J. Rouquerol, K.S.W. Sing, *Adsorption by Powders and Porous Solids: Principles, Methodology, and Applications*, Academic Press, San Diego, 1999.
- [20] A.R. Khataee, *Environ. Technol.* 30 (2009) 1155–1168.
- [21] M. Muruganandham, N. Shobana, M. Swaminathan, *J. Mol. Catal. A: Chem.* 246 (2006) 154–161.
- [22] I.K. Konstantinou, T.A. Albanis, *Appl. Catal. B* 49 (2004) 1–14.
- [23] N. Daneshvar, S. Aber, M.S.S. Dorraji, A.R. Khataee, M.H. Rasoulifard, *Int. J. Chem. Biol. Eng.* 1 (2008) 1307–7449.
- [24] M. Shirzad-Siboni, M. Farrokhi, R. Darvishi Cheshmeh Soltani, A. Khataee, S. Tajassosi, *Ind. Eng. Chem. Res.* 53 (2014) 1079–1087.
- [25] F. Ji, C. Li, J. Zhang, L. Deng, *J. Hazard. Mater.* 186 (2011) 1979–1984.
- [26] A.R. Khataee, M. Fathinia, S.W. Joo, *Spectrochim. Acta Part A* 112 (2013) 33–45.
- [27] T.A. Gad-Allah, S. Kato, S. Satokawa, T. Kojima, *Desalination* 244 (2009) 1–11.